Progress In Electromagnetics Research, Vol. 138, 211–226, 2013

STRUCTURAL BEHAVIOR OF THE MUSIC-TYPE ALGORITHM FOR IMAGING PERFECTLY CONDUCTING CRACKS

Young-Deuk Joh and Won-Kwang Park*

Department of Mathematics, Kookmin University, Seoul 136-702, Korea

Abstract—We consider MUltiple SIgnal Classification (MUSIC)-type imaging of perfectly conducting cracks arising in inverse scattering problems. We first explore the structure of a MUSIC-type imaging function by finding a relationship between it and the Bessel function of order zero of the first kind. Then, we design multi-frequency based MUSIC-type imaging in order to improve the traditional one, and establish a relationship with the Bessel function of integer order of the first kind. Some numerical experiments are presented to support the results of our investigation.

1. INTRODUCTION

The inverse scattering problem for identification of the shape of perfectly conducting cracks is an interesting research topic in mathematics, physics, and various applied sciences. To the best of our knowledge, the two-dimensional inverse scattering problem from a perfectly conducting crack that satisfies Dirichlet boundary condition was first investigated in [19], where a Newton method is presented for determining the approximate shape of a crack based on the Fréchet derivative.

Generally, when performing a Newton-type iterative algorithm, a good initial guess that is close to the unknown target (here, a crack) must be applied in order to avoid the non-convergence or appearance of local minima. For this reason, various non-iterative shape reconstruction algorithms, such as linear sampling method [7, 8, 12, 18], topological derivative [2, 20, 24, 25], Kirchhoff and subspace migrations [3, 16, 17, 22, 23, 27], SAR imaging technique [9, 15, 32–35], and

Received 31 January 2013, Accepted 15 March 2013, Scheduled 20 March 2013

* Corresponding author: Won-Kwang Park (parkwk@kookmin.ac.kr).

MUltiple SIgnal Classification (MUSIC) [4, 5, 11, 26, 28], have been investigated.

Among these, the MUSIC-type algorithm has been shown to be feasible in various inverse scattering problems and generalized to the imaging of arbitrarily shaped targets in two- and three-dimensional problems. Related works can be found in [1, 6, 10, 14, 29, 31, 36, 37] and references therein. However, contrary to the theoretical evaluations, sometimes the MUSIC algorithm does not yield good results, or it generates unexpected artifacts that are similar in shape to the target of interest. Hence, a careful investigation of the mathematical properties of the MUSIC algorithm must be considered.

Motivated by the above, this paper addresses the identification of some properties of the MUSIC-type imaging algorithm in inverse scattering from perfectly conducting cracks at a fixed single frequency. For this purpose, we investigate a relationship between the MUSIC-type imaging function and the Bessel function of order zero of the first kind. This relationship leads to an explanation of why the MUSIC algorithm cannot be applied to the limited-view inverse scattering problems and why it generates some artifacts that are similar in shape to the crack(s). Based on this relationship, we analyze multi-frequency based MUSIC algorithm and discover a relationship with the Bessel function of integer order of the first kind. This result explains why multi-frequency MUSIC algorithm is an improvement on the traditional one.

This paper is organized as follows. In Section 2, we briefly survey the two-dimensional direct scattering problem, far-field pattern, and MUSIC algorithm. In Section 3, we identify the structure of the MUSIC-type imaging function, and discuss its properties, and then introduce a multi-frequency MUSIC imaging function, and discover its structure. Some numerical experiments are shown in Section 4. In Section 5, our conclusions are briefly presented.

2. DIRECT SCATTERING PROBLEM AND MUSIC ALGORITHM

In this section, we briefly survey the two-dimensional direct scattering problem for the existence of perfectly conducting cracks, and the MUSIC algorithm. A more detailed discussion can be found in [19, 26].

2.1. Two-dimensional Direct Scattering Problem

First, we consider the two-dimensional electromagnetic scattering by a perfectly conducting crack, Γ, located in the space $\mathbb{R}^2$. Assume that

the crack is a smooth, nonintersecting curve, that can be represented as

$$\Gamma = \{\phi(t) : t \in [-1, 1]\}$$

where $\phi[-1, 1] \longrightarrow \mathbb{R}^2$ is an injective piecewise smooth function.

In this paper, we consider only the Transverse Magnetic (TM) polarization case. Let $u(\mathbf{x})$ be the time-harmonic total field that satisfies the two-dimensional Helmholtz equation

$$\begin{cases} \Delta u(\mathbf{x}) + k^2 u(\mathbf{x}) = 0 & \text{in} \quad \mathbb{R}^2 \backslash \Gamma \\ u(\mathbf{x}) = 0 & \text{on} \quad \Gamma \end{cases} \tag{1}$$

with a positive wavenumber k. It should be noted the total field can be decomposed as

$$u(\mathbf{x}) = u_{\text{inc}}(\mathbf{x}) + u_{\text{scat}}(\mathbf{x}),$$

where $u_{\text{inc}}(\mathbf{x}) = \exp(jk\boldsymbol{\theta} \cdot \mathbf{x})$ is the given incident field with incident direction $\boldsymbol{\theta} \in \mathbb{S}^1$ (unit circle), and $u_{\text{scat}}(\mathbf{x})$ is the unknown scattered field that satisfies the Sommerfeld radiation condition

$$\lim_{|\mathbf{x}| \to \infty} \sqrt{|\mathbf{x}|} \left(\frac{\partial u_{\text{scat}}(\mathbf{x})}{\partial |\mathbf{x}|} - jk u_{\text{scat}}(\mathbf{x}) \right) = 0$$

uniformly in all directions $\hat{\mathbf{x}} = \frac{\mathbf{x}}{|\mathbf{x}|}$.

According to the result in [19], $u_{\text{scat}}(\mathbf{x})$ can be represented as a single-layer potential with unknown density $\varphi(\mathbf{y}; \boldsymbol{\theta})$

$$u_{\text{scat}}(\mathbf{x}) = \int_{\Gamma} \Phi(\mathbf{x}, \mathbf{y}) \varphi(\mathbf{y}; \boldsymbol{\theta}) d\mathbf{y} \quad \text{for} \quad \mathbf{x} \in \mathbb{R}^2 \backslash \Gamma,$$

where Φ is the two-dimensional fundamental solution of the Helmholtz equation

$$\Phi(\mathbf{x}, \mathbf{y}) = -\frac{j}{4} H_0^1(k|\mathbf{x} - \mathbf{y}|) \quad \text{for} \quad \mathbf{x} \neq \mathbf{y}. \tag{2}$$

Here, H_0^1 denotes the Hankel function of order zero and of the first kind. The far-field pattern $u_\infty(\hat{\mathbf{x}}; \boldsymbol{\theta})$ of the scattered field $u_{\text{scat}}(\mathbf{x})$ is defined on $\mathbb{S}^1$ such that

$$u_{\text{scat}}(\mathbf{x}) = \frac{\exp(jk|\mathbf{x}|)}{\sqrt{|\mathbf{x}|}} \left\{ u_\infty(\hat{\mathbf{x}}; \boldsymbol{\theta}) + O\left(\frac{1}{|\mathbf{x}|} \right) \right\}$$

uniformly in all directions $\hat{x} = \frac{x}{|\mathbf{x}|}$ and $|\mathbf{x}| \longrightarrow \infty$. From the above representation and the asymptotic formula for (2), the far field pattern is given by

$$u_\infty(\hat{\mathbf{x}}; \boldsymbol{\theta}) = -\frac{\exp(j\pi/4)}{\sqrt{8\pi k}} \int_{\Gamma} \exp(-jk\hat{\mathbf{x}} \cdot \mathbf{y}) \varphi(\mathbf{y}; \boldsymbol{\theta}) d\mathbf{y}. \tag{3}$$

2.2. MUSIC-type Imaging Function: An Introduction

Next, we introduce the traditional MUSIC-type algorithm for imaging of cracks. For the sake of simplicity, we exclude the constant $-\frac{\exp(j\pi/4)}{\sqrt{8\pi k}}$ from formula (3).

Throughout this paper, we assume that the crack is divided into M different segments of size of the order of half the wavelength $\frac{\lambda}{2}$. Bearing in mind the Rayleigh resolution limit for far-field data, only one point at each segment is expected to contribute at the image space of the response matrix $\mathbb{K}$ (see [1, 5, 26, 28] for instance). Each of these points, say, $\mathbf{y}_m$ for $m = 1, 2, \ldots, M$, can be imaged via the MUSIC-type algorithm. Based on this assumption, let us consider the following Singular Value Decomposition (SVD) of the Multi-Static Response (MSR) matrix $\mathbb{K} = [u_\infty(\hat{\mathbf{x}}_p; \boldsymbol{\theta}_q)]_{p,q=1}^N \in \mathbb{C}^{N\times N}$:

$$\mathbb{K} = \sum_{m=1}^{M} \sigma_m \mathbf{U}_m \mathbf{V}_m^*, \tag{4}$$

where superscript $*$ is the mark of Hermitian, $\mathbf{U}_m$ and $\mathbf{V}_m \in \mathbb{C}^{N\times 1}$ are respectively the left- and right-singular vectors of $\mathbb{K}$, and σ_m denotes singular values that satisfy

$$\sigma_1 \geq \sigma_2 \geq \ldots \geq \sigma_M > 0 \quad \text{and} \quad \sigma_m = 0 \quad \text{for} \quad m \geq M+1.$$

Then, $\{\mathbf{U}_1, \mathbf{U}_2, \ldots, \mathbf{U}_M\}$ and $\{\mathbf{U}_{M+1}, \mathbf{U}_{M+2}, \ldots, \mathbf{U}_N\}$, are the basis for the signal and null (or noise) space of $\mathbb{K}$, respectively. Therefore, one can define the projection operator onto the null (or noise) subspace, $\mathbf{P}_N$: $\mathbb{C}^{N\times 1} \longrightarrow \mathbb{C}^{N\times 1}$. This projection is given explicitly by

$$\mathbf{P}_N := \mathbb{I}_N - \sum_{m=1}^{M} \mathbf{U}_m \mathbf{U}_m^*, \tag{5}$$

where $\mathbb{I}_N$ denotes the $N \times N$ identity matrix. For any point $\mathbf{z} \in \mathbb{R}^2$, we define a test vector $\mathbf{f}(\mathbf{z}) \in \mathbb{C}^{N\times 1}$ as

$$\mathbf{f}(\mathbf{z}) = \left[\exp(jk\boldsymbol{\theta}_1 \cdot \mathbf{z}), \exp(jk\boldsymbol{\theta}_2 \cdot \mathbf{z}), \ldots, \exp(jk\boldsymbol{\theta}_N \cdot \mathbf{z})\right]^T.$$

Then, it can be shown that there exists $N_0 \in \mathbb{N}$ such that for any $N \geq N_0$, the following statement holds (see [1, 5, 11, 26, 28]):

$$\mathbf{f}(\mathbf{z}) \in \text{Range}(\mathbb{K}\overline{\mathbb{K}}) \quad \text{if and only if} \quad z \in \{\mathbf{y}_1, \mathbf{y}_2, \ldots, \mathbf{y}_M\}.$$

Using this, we can design a MUSIC-type imaging function W: $\mathbb{C}^{N\times 1} \longrightarrow \mathbb{R}$ such that

$$W(\mathbf{z}) = |\mathbf{P}_N(\mathbf{f}(\mathbf{z}))|^{-1} = \frac{1}{|\mathbf{P}_N(\mathbf{f}(\mathbf{z}))|}. \tag{6}$$

Then, the map of $W(\mathbf{z})$ will have peaks of large and small magnitudes at $\mathbf{z} \in \Gamma$ and $\mathbf{z} \in \mathbb{R}^2 \backslash \Gamma$, respectively.

3. STRUCTURE ANALYSIS OF MUSIC-TYPE IMAGING FUNCTION

In order to perform an analysis of MUSIC-type imaging, we introduce two lemmas derived in [3] and [13].

Lemma 3.1 (see [3]). *For $\boldsymbol{\theta}_n \in \mathbb{S}^1$, define $\mathbf{D}(\boldsymbol{y}) \in \mathbb{C}^{N\times 1}$ as*

$$\mathbf{D}(\mathbf{y}) = \left[\exp(jk\boldsymbol{\theta}_1 \cdot \mathbf{y}), \exp(jk\boldsymbol{\theta}_2 \cdot \mathbf{y}), \ldots, \exp(jk\boldsymbol{\theta}_N \cdot \mathbf{y})\right]^T.$$

Then, the left singular vectors $\mathbf{U}_m$ of the MSR matrix $\mathbb{K}$ is of the form

$$\mathbf{U}_m \approx \frac{\mathbf{D}(\mathbf{y}_m)}{|\mathbf{D}(\mathbf{y}_m)|} = \frac{\mathbf{D}(\mathbf{y}_m)}{\sqrt{N}} \tag{7}$$

for $m = 1, 2, \ldots, M$.

Lemma 3.2 (see [13]). *For sufficiently large N, $\boldsymbol{\theta}_n \in \mathbb{S}^1$, and $\boldsymbol{y} \in \mathbb{R}^2$, the following relationship holds:*

$$\frac{1}{N}\sum_{n=1}^{N} \exp(jk\boldsymbol{\theta}_n \cdot \mathbf{y}) \approx \frac{1}{2\pi}\int_{\mathbb{S}^1} \exp(jk\boldsymbol{\theta} \cdot \mathbf{y}) dS(\boldsymbol{\theta}) = J_0(k|\mathbf{y}|).$$

3.1. Single-frequency MUSIC-type Imaging

Now, we explore the structure of the traditional MUSIC-type imaging function (6). For the sake of simplicity, we assume that the incident and observation direction configurations are same, i.e., $\hat{\mathbf{x}}_p = -\boldsymbol{\theta}_p$, for $p = 1, 2, \ldots, N$. Then, based on Lemmas 3.1 and 3.2, we can obtain the following structure of MUSIC-type imaging function.

Theorem 3.3 *For sufficiently large N and k, $W(\boldsymbol{z})$ of (6) is of the form:*

$$W(\mathbf{z}) = \frac{1}{|\mathbf{P}_N(\mathbf{f}(\mathbf{z}))|} \approx \frac{1}{\sqrt{N}}\left(1 - \sum_{m=1}^{M} J_0(k|\mathbf{z} - \mathbf{y}_m|)^2\right)^{-1/2},$$

where $J_n(\cdot)$ denotes the Bessel function of integer order n of the first kind.

Proof. Applying Lemma 3.1, we can evaluate the following

$$\mathbf{P}_N(\mathbf{f}(\mathbf{z})) = \left(\mathbb{I} - \sum_{m=1}^{M} \mathbb{U}_m \mathbb{U}_m^*\right)\mathbf{f}(\mathbf{z}) = \begin{bmatrix} \exp(jk\boldsymbol{\theta}_1 \cdot \mathbf{z}) \\ \exp(jk\boldsymbol{\theta}_2 \cdot \mathbf{z}) \\ \vdots \\ \exp(jk\boldsymbol{\theta}_N \cdot \mathbf{z}) \end{bmatrix} - \sum_{m=1}^{M} \frac{\mathbb{A}}{N},$$

where $\mathbb{A} \in \mathbb{C}^{N\times 1}$ is defined as

$$\mathbb{A} := \begin{bmatrix} \exp(jk\boldsymbol{\theta}_1 \cdot \mathbf{z}) + \sum_{n\in\mathbb{N}_1} \exp\Big(jk(\boldsymbol{\theta}_1 \cdot \mathbf{y}_m + \boldsymbol{\theta}_n \cdot (\mathbf{z}-\mathbf{y}_m))\Big) \\ \exp(jk\boldsymbol{\theta}_2 \cdot \mathbf{z}) + \sum_{n\in\mathbb{N}_2} \exp\Big(jk(\boldsymbol{\theta}_2 \cdot \mathbf{y}_m + \boldsymbol{\theta}_n \cdot (\mathbf{z}-\mathbf{y}_m))\Big) \\ \vdots \\ \exp(jk\boldsymbol{\theta}_N \cdot \mathbf{z}) + \sum_{n\in\mathbb{N}_N} \exp\Big(jk(\boldsymbol{\theta}_N \cdot \mathbf{y}_m + \boldsymbol{\theta}_n \cdot (\mathbf{z}-\mathbf{y}_m))\Big) \end{bmatrix}.$$

Here, the set $\mathbb{N}_p$ is defined as follows: for $p = 1, 2, \ldots, N$,

$$\mathbb{N}_p := \{1, 2, \ldots, N\}\backslash\{p\}.$$

Note that since

$$\exp(jk\boldsymbol{\theta}_p \cdot \mathbf{z}) = \exp(jk\boldsymbol{\theta}_p \cdot \mathbf{y}_m) \exp\Big(jk\boldsymbol{\theta}_p \cdot (\mathbf{z}-\mathbf{y}_m)\Big),$$

we can observe that for $p = 1, 2, \ldots, N$,

$$\begin{aligned} & \frac{1}{N}\sum_{m=1}^{M}\left(\exp(jk\boldsymbol{\theta}_p \cdot \mathbf{z}) + \sum_{n\in\mathbb{N}_p} \exp\Big(jk(\boldsymbol{\theta}_p \cdot \mathbf{y}_m + \boldsymbol{\theta}_n \cdot (\mathbf{z}-\mathbf{y}_m))\Big)\right) \\ = & \frac{1}{N}\sum_{m=1}^{M}\left(\exp(jk\boldsymbol{\theta}_p \cdot \mathbf{y}_m)\sum_{n=1}^{N}\exp\Big(jk\boldsymbol{\theta}_n \cdot (\mathbf{z}-\mathbf{y}_m)\Big)\right) \\ = & \sum_{m=1}^{M}\exp(jk\boldsymbol{\theta}_p \cdot \mathbf{y}_m) J_0(k|\mathbf{z}-\mathbf{y}_m|). \end{aligned}$$

Hence,

$$\mathbf{P}_N(\mathbf{f}(\mathbf{z})) = \begin{bmatrix} \exp(jk\boldsymbol{\theta}_1 \cdot \mathbf{z}) - \sum_{m=1}^{M}\exp(jk\boldsymbol{\theta}_1 \cdot \mathbf{y}_m) J_0(k|\mathbf{z}-\mathbf{y}_m|) \\ \exp(jk\boldsymbol{\theta}_2 \cdot \mathbf{z}) - \sum_{m=1}^{M}\exp(jk\boldsymbol{\theta}_2 \cdot \mathbf{y}_m) J_0(k|\mathbf{z}-\mathbf{y}_m|) \\ \vdots \\ \exp(jk\boldsymbol{\theta}_N \cdot \mathbf{z}) - \sum_{m=1}^{M}\exp(jk\boldsymbol{\theta}_N \cdot \mathbf{y}_m) J_0(k|\mathbf{z}-\mathbf{y}_m|) \end{bmatrix}.$$

With this, we arrive

$$\begin{aligned}|\mathbf{P}_N(\mathbf{f}(\mathbf{z}))| &= \left(\mathbf{P}_N(\mathbf{f}(\mathbf{z}))\overline{\mathbf{P}_N(\mathbf{f}(\mathbf{z}))}\right)^{1/2} \\ &= \left(\sum_{n=1}^{N}\left(1-(\Lambda_1+\overline{\Lambda}_1)+(\Lambda_2\overline{\Lambda}_2)\right)\right)^{1/2},\end{aligned}$$

where $\overline{\Lambda}$ denotes the complex conjugate of Λ and

$$\begin{aligned}\Lambda_1 &:= \sum_{m=1}^{M}\exp(jk\boldsymbol{\theta}_n\cdot(\mathbf{z}-\mathbf{y}_m))J_0(k|\mathbf{z}-\mathbf{y}_m|) \\ \Lambda_2 &:= \sum_{m=1}^{M}\exp(jk\boldsymbol{\theta}_n\cdot\mathbf{y}_m)J_0(k|\mathbf{z}-\mathbf{y}_m|).\end{aligned}$$

Applying Lemma 3.2, we can evaluate

$$\begin{aligned}\sum_{n=1}^{N}\Lambda_1 &= \sum_{n=1}^{N}\sum_{m=1}^{M}\exp(jk\boldsymbol{\theta}_n\cdot(\mathbf{z}-\mathbf{y}_m))J_0(k|\mathbf{z}-\mathbf{y}_m|) \\ &= \sum_{m=1}^{M}\left(\sum_{n=1}^{N}\exp(jk\boldsymbol{\theta}_n\cdot(\mathbf{z}-\mathbf{y}_m))\right)J_0(k|\mathbf{z}-\mathbf{y}_m|) \\ &= N\sum_{m=1}^{M}J_0(k|\mathbf{z}-\mathbf{y}_m|)^2, \qquad (8)\end{aligned}$$

and similarly

$$\sum_{n=1}^{N}\overline{\Lambda}_1 = N\sum_{m=1}^{M}J_0(k|\mathbf{z}-\mathbf{y}_m|)^2. \qquad (9)$$

Based on the orthonormal property of singular vectors, we can observe that

$$\begin{aligned}\mathbf{U}_p\mathbf{U}_q^* &= \frac{1}{N}\sum_{n=1}^{N}\exp(jk\theta_n\cdot(\mathbf{y}_p-\mathbf{y}_q)) = J_0(k|\mathbf{y}_p-\mathbf{y}_q|) \\ &\approx \sqrt{\frac{2}{\pi k|\mathbf{y}_p-\mathbf{y}_q|}}\cos\left(k|\mathbf{y}_p-\mathbf{y}_q|-\frac{\pi}{4}\right)\longrightarrow 0 \qquad (10)\end{aligned}$$

for $p\neq q$ and sufficiently large k. Applying this property (10), we can observe that

$$\Lambda_2\overline{\Lambda}_2=\sum_{p=1}^{M}\sum_{q=1}^{M}\exp(jk\theta_n\cdot\mathbf{y}_p)J_0(k|\mathbf{z}-\mathbf{y}_p|)\exp(-jk\theta_n\cdot\mathbf{y}_q)J_0(k|\mathbf{z}-\mathbf{y}_q|).$$

Hence, applying Lemma 3.2 yields

$$\sum_{n=1}^{N} \Lambda_2 \overline{\Lambda}_2 = \sum_{n=1}^{N} \sum_{p=1}^{M} \sum_{q=1}^{M} \exp(jk\theta_n \cdot (\mathbf{y}_p - \mathbf{y}_q)) J_0(k|\mathbf{z} - \mathbf{y}_p|) J_0(k|\mathbf{z} - \mathbf{y}_q|)$$
$$= N \sum_{p=1}^{M} \sum_{q=1}^{M} J_0(k|\mathbf{y}_p - \mathbf{y}_q|) J_0(k|\mathbf{z} - \mathbf{y}_p|) J_0(k|\mathbf{z} - \mathbf{y}_q|).$$

If $p \neq q$, then by property (10), $J_0(k|\mathbf{y}_p - \mathbf{y}_q|) = 0$. If $p = q$, then since $J_0(0) = 1$, we can obtain

$$\sum_{n=1}^{N} \Lambda_2 \overline{\Lambda}_2 = N \sum_{m=1}^{M} J_0(k|\mathbf{z} - \mathbf{y}_m|)^2. \tag{11}$$

Therefore, by (8), (9), and (11), we can obtain

$$|\mathbf{P}_N(\mathbf{f}(\mathbf{z}))| = \sqrt{N} \left(1 - \sum_{m=1}^{M} J_0(k|\mathbf{z} - \mathbf{y}_m|)^2 \right)^{1/2}.$$

This ends the proof.

Note that $J_0(x)^2$ has the maximum value 1 at $x = 0$. This is the reason why the map of $|\mathbf{P}_N(\mathbf{f}(\mathbf{z}))|$ plots magnitude ∞ at $\mathbf{z} = \mathbf{y}_m \in \Sigma_m$. Moreover, the oscillating property of $J_0(x)^2$ tells why imaging function (6) plots artifacts similar to the shape of crack(s). Hence, this oscillating pattern of the Bessel function must be reduced or eliminated in order to improve the imaging performance. One way to do so is to apply $k = +\infty$ in theory. Another way is to apply several frequencies to the imaging function (6).

3.2. Multi-frequency MUSIC-type Imaging

Now, we consider multi-frequency MUSIC-type imaging in order to improve the traditional single-frequency one. For given $S-$ different wavenumbers $0 < k_1 < k_2 < \ldots < k_S$, we collect MSR matrix $\mathbb{K}(k_s)$ and then perform SVD as

$$\mathbb{K}(k_s) = \sum_{m=1}^{M} \sigma_m(k_s) \mathbb{U}(k_s) \mathbb{V}(k_s).$$

Then, by Lemma 3.1, singular vectors $\mathbf{U}_m(k_s) \in \mathbb{C}^{N \times 1}$ are given by

$$\mathbf{U}_m(k_s) \approx \frac{1}{\sqrt{N}} \left[\exp(jk_s \boldsymbol{\theta}_1 \cdot \mathbf{y}), \exp(jk_s \boldsymbol{\theta}_2 \cdot \mathbf{y}), \ldots, \exp(jk_s \boldsymbol{\theta}_N \cdot \mathbf{y}) \right]^T.$$

Let us choose a test vector $\mathbf{f}(\mathbf{z}, k_s) \in \mathbb{C}^{N\times 1} \times \mathbb{R}$ as

$$\mathbf{f}(\mathbf{z}, k_s) = \left[\exp(jk_s\boldsymbol{\theta}_1 \cdot \mathbf{z}), \exp(jk_s\boldsymbol{\theta}_2 \cdot \mathbf{z}), \ldots, \exp(jk_s\boldsymbol{\theta}_N \cdot \mathbf{z})\right]^T,$$

and define projection operator $\mathbf{P}_N : \mathbb{C}^{N\times 1} \times \mathbb{R} \longrightarrow \mathbb{C}^{N\times 1}$ as

$$\mathbf{P}_N(\mathbf{f}(\mathbf{z}, k_s)) = \left(\mathbb{I} - \sum_{m=1}^{M} \mathbf{U}_m(s)\mathbf{U}_m^*(s)\right)\mathbf{f}(\mathbf{z}, k_s).$$

With this, we introduce a multi-frequency based MUSIC-type imaging function $W_{MF} : \mathbb{C}^{N\times 1} \times \mathbb{N} \longrightarrow \mathbb{R}$ defined by

$$W_{MF}(\mathbf{z}; S) = \left(\frac{1}{S}\sum_{s=1}^{S} |\mathbf{P}_N(\mathbf{f}(\mathbf{z}, k_s))|^2\right)^{-1/2}$$

then, based on Theorem 3.3, we can obtain the following result.

Theorem 3.4 *Assume that k_S and S are sufficiently large; then,*

$$W_{MF}(\mathbf{z}; S) \approx \sqrt{\frac{1}{N}}\left(1 - \sum_{m=1}^{M} \Psi(|\mathbf{z} - \mathbf{y}_m|; k_1, k_S)\right)^{-1/2},$$

where function $\Psi(t; k_1, k_S)$ is defined as

$$\Psi(t; k_1, k_S) : = \frac{k_S}{k_S - k_1}\left(J_0(k_S t)^2 + J_1(k_S t)^2\right) - \frac{k_1}{k_S - k_1}\left(J_0(k_1 t)^2 + J_1(k_1 t)^2\right) + \int_{k_1}^{k_S} J_1(k|\mathbf{y} - \mathbf{y}_m|)^2 dk. \quad (12)$$

Proof. According to the result in Theorem 3.3, we can calculate

$$\begin{aligned}\frac{1}{S}\sum_{s=1}^{S} |\mathbf{P}_N(\mathbf{f}(\mathbf{z}, k_s))|^2 &\approx \frac{1}{S}\sum_{s=1}^{S} N\left(1 - \sum_{m=1}^{M} J_0(k_s|\mathbf{z} - \mathbf{y}_m|)^2\right) \\ &= \frac{N}{S}\left(S - \sum_{m=1}^{M}\sum_{s=1}^{S} J_0(k_s|\mathbf{z} - \mathbf{y}_m|)^2\right) \\ &\approx N\left(1 - \sum_{m=1}^{M} \frac{1}{k_S - k_1}\int_{k_1}^{k_S} J_0(k|\mathbf{y} - \mathbf{y}_m|)^2 dk\right). \quad (13)\end{aligned}$$

Then applying an indefinite integral of the Bessel function (see [30, Page 35])

$$\int J_0(x)^2 dx = x\left(J_0(x)^2 + J_1(x)^2\right) + \int J_1(x)^2 dx$$

yields

$$\int_{k_1}^{k_S} J_0(k|\mathbf{y}-\mathbf{y}_m|)^2 dk = k_S\Big(J_0(k_S|\mathbf{y}-\mathbf{y}_m|)^2 + J_1(k_S|\mathbf{y}-\mathbf{y}_m|)^2\Big) - k_1\Big(J_0(k_1|\mathbf{y}-\mathbf{y}_m|)^2 + J_1(k_1|\mathbf{y}-\mathbf{y}_m|)^2\Big) + \int_{k_1}^{k_S} J_1(k|\mathbf{y}-\mathbf{y}_m|)^2 dk. \quad (14)$$

Hence, by combining (13) and (14), we can obtain

$$\sum_{s=1}^{S} |\mathbf{P}_N(\mathbf{f}(\mathbf{z},k_s))|^2 \approx N\left(1 - \sum_{m=1}^{M} \Psi(|\mathbf{y}-\mathbf{y}_m|;k_1,k_S)\right)$$

Therefore,

$$W_{MF}(\mathbf{z};S) \approx \sqrt{\frac{1}{N}}\left(1 - \sum_{m=1}^{M} \Psi(|\mathbf{z}-\mathbf{y}_m|;k_1,k_S)\right)^{-1/2}.$$

This completes the proof.

Based on Lemmas 3.1 and 3.2, and Theorems 3.3 and 3.4, we can examine some properties of the MUSIC-type imaging algorithm. They can be summarized as follows.

(i) The total value of the incident and observation direction N must be sufficiently large. This is why some unexpected replicas appeared in the map of $W(\mathbf{z})$ with a small number N (see [28, Figure 7]).

(ii) The set of directions $\{\boldsymbol{\theta}_n\}_{n=1}^{N}$ must span the unit circle $\mathbb{S}^1$. This means that the MUSIC algorithm yields a good result in full-view inverse scattering problems and a poor result in limited-view problems (see [4, 23]).

(iii) $J_0(x)$ reaches its maximum value 1 at $x = 0$. This means that for a nonzero wavenumber k, the map of $W(\mathbf{z})$ will have plots of large magnitude (almost ∞ in theory) at $\mathbf{z} = \mathbf{y}_m \in \Gamma$ for $m = 1, 2, \ldots, M$, and small magnitude (almost zero in theory) at $\mathbf{z} \notin \Gamma$. However, due to the oscillation property of the Bessel function, some artifacts of small magnitude are displayed.

(iv) According to the recent work [17], the last term of (12) can be negligible. Since $\Psi(x;k_1,k_S)$ reaches its maximum value 1 at $x = 0$ for any nonzero wavenumbers k_1 and k_S, the map of $W_{MF}(\mathbf{z};S)$ has properties similar to those of $W(\mathbf{z})$, except for less oscillation. Hence, the map of $W_{MF}(\mathbf{z};S)$ should offer a better result than that of $W(\mathbf{z})$, i.e., the multi-frequency MUSIC algorithm successfully improves the traditional one.

4. NUMERICAL EXAMPLES

In order to verify Theorems 3.3 and 3.4, we present some numerical examples. We apply a wavenumber of the form $k_s = \frac{2\pi}{\lambda_s}$; where λ_s, $s = 1, 2, \ldots, S(= 10)$, is the given wavelength. Here, k_s are always equi-distributed in the interval $[k_1, k_S]$. For mapping the $W(\mathbf{z})$, the applied wavelength is k_S. The observation directions $\boldsymbol{\theta}_n$ are taken as

$$\boldsymbol{\theta}_n = \left[\cos\frac{2\pi n}{N}, \sin\frac{2\pi n}{N}\right]^T.$$

To illustrate crack, three Γ_l are chosen:

$$\Gamma_1 = \left\{\left[s, \frac{1}{2}\cos\frac{s\pi}{2} + \frac{1}{5}\sin\frac{s\pi}{2} - \frac{1}{10}\cos\frac{3s\pi}{2}\right]^T : s \in [-1, 1]\right\},$$

$$\Gamma_2 = \left\{\left[2\sin\frac{s}{2}, \sin s\right]^T : s \in \left[\frac{\pi}{4}, \frac{7\pi}{4}\right]\right\},$$

$$\Gamma_3 = \Gamma_3^{(1)} \cup \Gamma_3^{(2)},$$

where

$$\Gamma_3^{(1)} = \left\{\left[s - \frac{1}{5}, -\frac{s^2}{2} + \frac{3}{5}\right]^T : s \in \left[-\frac{1}{2}, \frac{1}{2}\right]\right\},$$

$$\Gamma_3^{(2)} = \left\{\left[s + \frac{1}{5}, s^3 + s^2 - \frac{3}{5}\right]^T : s \in \left[-\frac{1}{2}, \frac{1}{2}\right]\right\}.$$

All the far-field data $u_\infty(\hat{\mathbf{x}}_p; \boldsymbol{\theta}_q)$ of (3) are generated by a formulation involving the solution of a second-kind Fredholm integral equation along Γ_l, refer to [21, Chapter 3] and [21, Chapter 4] for single and multiple cracks, respectively. After generating the data, a 20 dB Gaussian random noise is added to the unperturbed data to show the robustness of the proposed algorithm. In order to obtain the number of nonzero singular values M_f for each frequency, a 0.1-threshold scheme (choosing first m singular values σ_m such that $\sigma_m/\sigma_1 \geq 0.1$) is adopted. A more detailed discussion of thresholding can be found in [26, 28].

First, we consider the imaging result of Γ_1 exhibited in Figure 1(a). In this example, we applied $N = 24$ directions and wavelengths $\lambda_1 = 0.6$ and $\lambda_{10} = 0.4$. As we expected in Theorem 3.3, peaks of large magnitude appear along Γ_1 and artifacts of small magnitude in the exterior of Γ_1 as well. Note that, based on Figure 1(b), these peaks of small magnitude can be eliminated by applying multiple frequencies. This result supports Theorem 3.4.

Next, we consider the result of Γ_2. In this example, $N = 64$ directions, and $\lambda_1 = 0.7$ and $\lambda_{10} = 0.5$ wavelengths are used. Similar to Figure 1, the shape of Γ_2 is well-reconstructed, but some replicas also appeared in Figure 2(a). Fortunately, applying multiple frequencies yields a more accurate result (see Figure 2(b)).

Figure 3 shows the application of the MUSIC algorithm for the imaging of multiple cracks Γ_3 with $N = 64$ directions and wavelengths $\lambda_1 = 0.5$ and $\lambda_{10} = 0.3$. Similar to Figures 1 and 2, we can conclude that peaks of large magnitude appear along the cracks, and that the multi-frequency MUSIC algorithm successfully improves the single-frequency one.

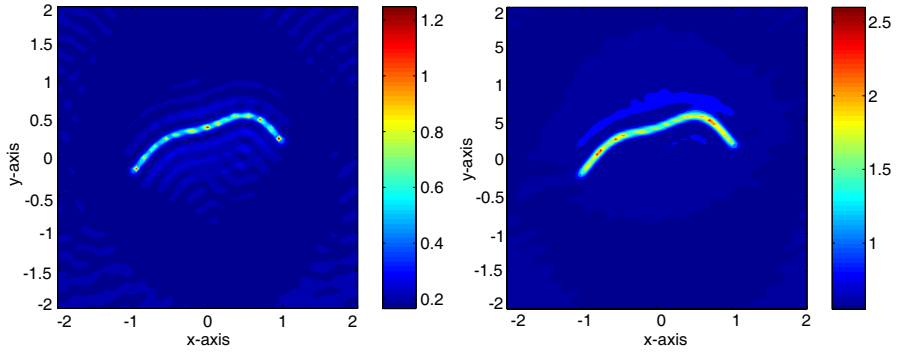

Figure 1. Shape reconstruction of Γ_1. (a) Map of $W(\mathbf{z})$. (b) Map of $W_{MF}(\mathbf{z}; 10)$.

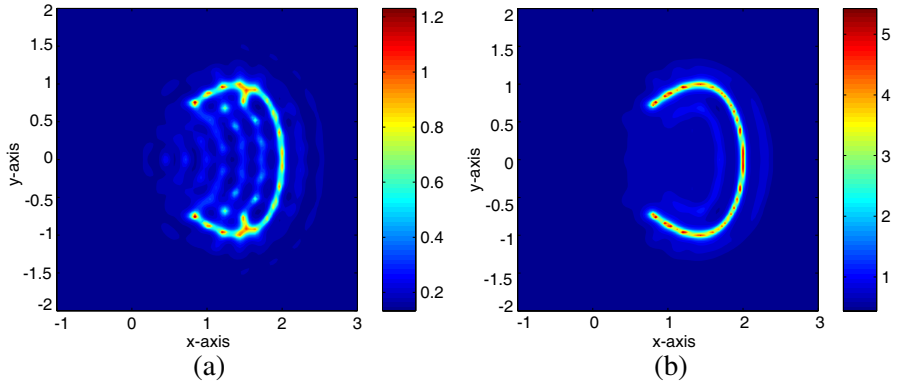

Figure 2. Shape reconstruction of Γ_2. (a) Map of $W(\mathbf{z})$. (b) Map of $W_{MF}(\mathbf{z}; 10)$.

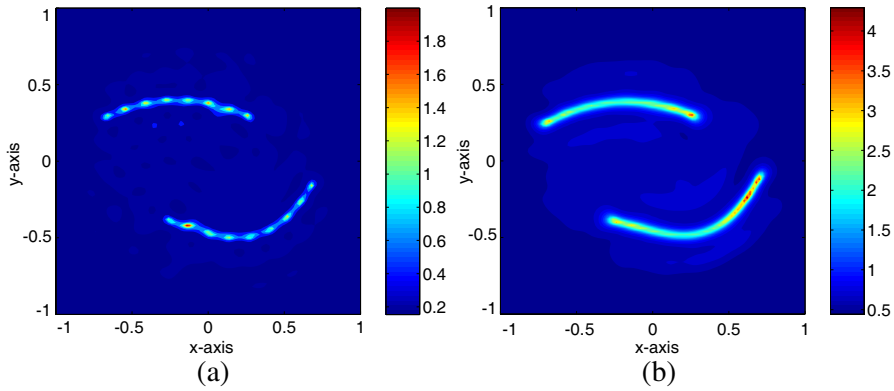

Figure 3. Shape reconstruction of Γ_3. (a) Map of $W(\mathbf{z})$. (b) Map of $W_{MF}(\mathbf{z}; 10)$.

5. CONCLUSION

Based on the indefinite integral of the Bessel function, we determined the structure of the MUSIC-type imaging function. Owing to the oscillation aspect of the Bessel function of integer order, we investigated why unexpected artifacts appear in the image via the MUSIC algorithm. This fact motivated us to propose a multi-frequency MUSIC algorithm. It was confirmed that this algorithm successfully improves the traditional algorithm.

We considered the MUSIC algorithm in full-view inverse scattering problem. It is well-known that the MUSIC algorithm cannot be applied to limited-view problems (see [4, 23]). In order to determine the structure of imaging functions in the limited-view configuration, the integration in Lemma 3.2 on the subset of a unit circle must be evaluated. Unfortunately, this evaluation is very difficult to perform. Therefore, identifying the structure of the MUSIC-type imaging function in the limited-view problem will be an interesting subject.

Finally, we considered the imaging function for the TM-polarization case. The extension of our study to the Transverse Electric (TE) polarization case (Neumann boundary condition) will be a forthcoming work.

ACKNOWLEDGMENT

Won-Kwang Park would like to thank Habib Ammari for much valuable advice. This work was supported by the research program of Kookmin

University in Korea, and the Basic Science Research Program through the National Research Foundation of Korea (NRF) funded by the Ministry of Education, Science and Technology (No. 2012-0003207).

REFERENCES

1. Ammari, H., *Mathematical Modeling in Biomedical Imaging II: Optical, Ultrasound, and Opto-acoustic Tomographies*, Lecture Notes in Mathematics: Mathematical Biosciences Subseries, Vol. 2035, Springer-Verlag, Berlin, 2011.
2. Ammari, H., J. Garnier, V. Jugnon, and H. Kang, "Stability and resolution analysis for a topological derivative based imaging functional," *SIAM J. Control. Optim.*, Vol. 50, 48–76, 2012.
3. Ammari, H., J. Garnier, H. Kang, W.-K. Park, and K. Sϕlna, "Imaging schemes for perfectly conducting cracks," *SIAM J. Appl. Math.*, Vol. 71, 68–91, 2011.
4. Ammari, H., E. Iakovleva, and D. Lesselier, "A MUSIC algorithm for locating small inclusions buried in a half-space from the scattering amplitude at a fixed frequency," *SIAM Multiscale Modeling Simulation*, Vol. 3, 597–628, 2005.
5. Ammari, H., H. Kang, H. Lee, and W.-K. Park, "Asymptotic imaging of perfectly conducting cracks," *SIAM J. Sci. Comput.*, Vol. 32, 894–922, 2010.
6. Bencheikh, M. L. and Y. Wang, "Combined esprit-rootMUSIC for DOA-DOD estimation in polarimetric bistatic MIMO radar," *Progress In Electromagnetics Research Letters*, Vol. 22, 109–117, 2011.
7. Cakoni, F. and D. Colton, "The linear sampling method for cracks," *Inverse Problems*, Vol. 19, 279–95, 2003
8. Catapano, I., F. Soldovieri, and L. Crocco, "On the feasibility of the linear sampling method for 3D GPR surveys," *Progress In Electromagnetics Research*, Vol. 118, 185–203, 2011.
9. Chang, Y.-L., C.-Y. Chiang, and K.-S. Chen, "SAR image simulation with application to target recognition," *Progress In Electromagnetics Research*, Vol. 119, 35–57, 2011.
10. Chen, X. and Y. Zhong, "MUSIC electromagnetic imaging with enhanced resolution for small inclusions," *Inverse Problems*, Vol. 25, 015008, 2009.
11. Cheney, M., "The linear sampling method and the MUSIC algorithm," *Inverse Problems*, Vol. 17, 591–595, 2001.
12. Colton, D., H. Haddar, and P. Monk, "The linear sampling

method for solving the electromagnetic inverse scattering problem," *SIAM J. Sci. Comput.*, Vol. 24, 719–731, 2002.

13. Griesmaier, R., "Multi-frequency orthogonality sampling for inverse obstacle scattering problems," *Inverse Problems*, Vol. 27, 085005, 2011.
14. Gu, X. and Y. Zhang, "Resolution threshold analysis of MUSIC algorithm in radar range imaging," *Progress In Electromagnetics Research B*, Vol. 31, 297–321, 2011.
15. Hasar, U. C. and J. J. Barroso, "Retrieval approach for determination of forward and backward wave impedances of bianisotropic metamaterials," *Progress In Electromagnetics Research*, Vol. 112, 109–124, 2011.
16. Hou, S., K. Huang, K. Sϕlna, and H. Zhao, "A phase and space coherent direct imaging method," *J. Opt. Soc. Am.*, Vol. 125, 227–238, 2009.
17. Joh, Y.-D., Y. M. Kwon, J. Y. Huh, and W.-K. Park, "Structure analysis of single- and multi-frequency subspace migrations in inverse scattering problems," *Progress In Electromagnetics Research*, Vol. 136, 607–622, 2013.
18. Kirsch, A. and Ritter S., "A linear sampling method for inverse scattering from an open arc," *Inverse Problems*, Vol. 16, 89–105, 2000.
19. Kress, R., "Inverse scattering from an open arc," *Math. Methods Appl. Sci.*, Vol. 18, 267–293, 1995.
20. Ma, Y.-K., P.-S. Kim, and W.-K. Park, "Analysis of topological derivative function for a fast electromagnetic imaging of perfectly conducing cracks," *Progress In Electromagnetics Research*, Vol. 122, 311–325, 2012.
21. Nazarchuk, Z. T., *Singular Integral Equations in Diffraction Theory*, Karpenko Physicomechanical Institute, Ukrainian Academy of Sciences, Vol. 210, L'viv, 1994.
22. Park, W.-K., "Non-iterative imaging of thin electromagnetic inclusions from multi-frequency response matrix," *Progress In Electromagnetics Research*, Vol. 106, 225–241, 2010.
23. Park, W.-K., "On the imaging of thin dielectric inclusions buried within a half-space," *Inverse Problems*, Vol. 26, 074008, 2010.
24. Park, W.-K., "On the imaging of thin dielectric inclusions via topological derivative concept," *Progress In Electromagnetics Research*, Vol. 110, 237–252, 2010.
25. Park, W.-K., "Topological derivative strategy for one-step iteration imaging of arbitrary shaped thin, curve-like electromagnetic

inclusions," *J. Comput. Phys.*, Vol. 231, 1426–1439, 2012.

26. Park, W.-K. and D. Lesselier, "Electromagnetic MUSIC-type imaging of perfectly conducting, arc-like cracks at single frequency," *J. Comput. Phys.*, Vol. 228, 8093–8111, 2009.
27. Park, W.-K. and D. Lesselier, "Fast electromagnetic imaging of thin inclusions in half-space affected by random scatterers," *Waves Random Complex Media*, Vol. 22, 3–23, 2012.
28. Park, W.-K. and D. Lesselier, "MUSIC-type imaging of a thin penetrable inclusion from its far-field multi-static response matrix," *Inverse Problems*, Vol. 25, 075002, 2009.
29. Pouramadi, M., M. Nakhkash, and A. A. Tadion, "Application of Mdl criterion for microwave imaging by MUSIC algorithm," *Progress In Electromagnetics Research B*, Vol. 40, 261–278, 2012.
30. Rosenheinrich, W., *Tables of Some Indefinite Integrals of Bessel Functions*, 2003, http://www.fh-jena.de/∼rsh/Forschung/Stoer /besint.pdf.
31. Solimene, R., A. Dell'Aversano, and G. Leone, "Interferometric time reversal MUSIC for small scatterer localization," *Progress In Electromagnetics Research,* Vol. 131, 243–258, 2012.
32. Wei, S.-J., X.-L. Zhang, and J. Shi, "Linear array SAR imaging via compressed sensing," *Progress In Electromagnetics Research*, Vol. 117, 299–319, 2011.
33. Yang, M. and G. Zhang, "Unsupervised target detection in SAR images using scattering center model and mean shift clustering algorithm," *Progress In Electromagnetics Research Letters*, Vol. 35, 11–18, 2012.
34. Yu, L. and Y. Zhang, "A 3D target imaging algorithm based on two-pass circular SAR observations," *Progress In Electromagnetics Research*, Vol. 122, 341–360, 2012.
35. Zhang, M., Y. W. Zhao, H. Chen, and W.-Q. Jiang, "SAR imaging simulation for composite model of ship on dynamic ocean ccene," *Progress In Electromagnetics Research*, Vol. 113, 395–412, 2011.
36. Zhang, X., G. Feng, and D. Xu, "Blind direction of angle and time delay estimation algorithm for uniform linear array employing multi-invariance MUSIC," *Progress In Electromagnetics Research Letters*, Vol. 13, 11–20, 2010.
37. Zhang, W., A. Hoorfar, and L. Li, "Through-the-wall target localization with time reversal MUSIC method," *Progress In Electromagnetics Research*, Vol. 106, 75–89, 2010.